https://doi.org/10.20965/ijat.2020.p0208

Paper:

Development of Surface Roughness Generation Model for CFRTP Manufactured by LFT-D

Motoyuki Murashima[*,†], **Takaharu Murooka**[**], **Noritsugu Umehara**[*], **and Takayuki Tokoroyama**[*]

[*]Department of Micro-Nano Mechanical Science and Engineering, Graduate School of Engineering, Nagoya University
Furo-cho, Chikusa-ku, Nagoya, Aichi 464-8603, Japan
[†]Corresponding author, E-mail: motoyuki.murashima@mae.nagoya-u.ac.jp
[**]Department of Mechanical Science and Engineering, Graduate School of Engineering, Nagoya University, Nagoya, Japan
[Received July 28, 2019; accepted October 8, 2019]

In this study, we propose a new surface generation model for carbon fiber reinforced thermoplastics (CFRTP) manufactured by the long fiber thermoplastic-direct (LFT-D) method. CFRTP are considered to be a next-generation structural material because of their high productivity as well as high mechanical strength and lightness. Conversely, CFRTP have a rough surface, which does not meet the automotive outer panel standard of a "class A surface." In the present study, we establish a surface roughness generation model based on a thermal shrinkage mismatch of thermoplastic resin to carbon fiber and non-uniform carbon fiber distribution. Furthermore, we construct a surface roughness estimation formula based on the model. In the calculation, a cross-sectional image of CFRTP is divided into many vertical segments. Subsequently, the thermal shrinkage of each segment is calculated with a standard deviation, an average, and a probability density of the amount of carbon fiber in each segment. The surface roughness of the manufactured CFRTP was measured using a surface profilometer. The result showed that the arithmetic surface roughness increased with the volume fraction of carbon fiber. We applied the surface roughness calculation to cross-sectional images of the specimens. Consequently, the estimated surface roughness showed the same tendency, in which the surface roughness increased with the volume fraction of carbon fiber. The slope of a regression line of the estimated surface roughness with respect to the volume fraction was 0.010, which was almost the same (0.011) as the slope of a regression line of the measured surface roughness. Furthermore, the estimation formula using a thermal shrinkage effective depth of 395 μm was able to estimate the surface roughness within a 3% average error. Using the estimation formula, it was predicted that the surface roughness increased with the standard deviation of the amount of carbon fiber in a segment. To confirm the reliability of the model and the formula, we measured the standard deviation of the amount of carbon fiber in CFRTP specimens, showing that the trend for CFRTP specimens matched the estimated values.

Keywords: CFRTP, surface roughness, LFT-D, thermal shrinkage

1. Introduction

Recently, carbon fiber reinforced plastics (CFRP) have received increased attention. CFRP, with both high strength and lightness, incorporate carbon fibers (CFs), which are light in weight and have excellent mechanical strength, in the resin. Their specific strength is reported to be approximately 3.3 times that of ordinary steel material [1, 2]. Thanks to its unique properties, CFRP have been widely used in the aircraft industry [3–5]. Conversely, the automotive industry, faced with the need to further improve fuel efficiency [6–10], has been attempting to achieve this using light CFRP for car bodies and chassis. However, because ordinary CFRP, which is primarily made from thermosetting resin, take a long time to set and have high production costs [11], they have rarely been used for popular cars.

In this context, carbon fiber reinforced thermoplastics (CFRTP) have recently attracted increased attention as a new composite material that characteristically contains CFs in the thermoplastic resin; they have already been used for some car components [1]. While the thermosetting resin used for conventional CFRP takes a long time to cure, the thermoplastic resin used for CFRTP melts instantly at increased temperatures, so that it can impregnate the CFs and mold the resin as it is. Therefore, CFRTP are expected to be able to be pressmolded with the same high productivity as the steel plates that are currently press-formed into car body shapes.

In press-molding CFRTP, the long fiber thermoplastic-direct (LFT-D) method is considered to be a next-generation molding technique because of its high productivity [12–16]. With the LFT-D technique, molten resin and CFs are continuously drawn into the kneading screws and are kneaded [17]. A kneaded body in a molten condition called a strand is heated with a heater and is arranged on the heated press mold. Next, the kneaded body is press-molded and is released from the mold in its high-temperature state. Finally, the molded body is cooled into a finished CFRTP product. The LFT-D technique using

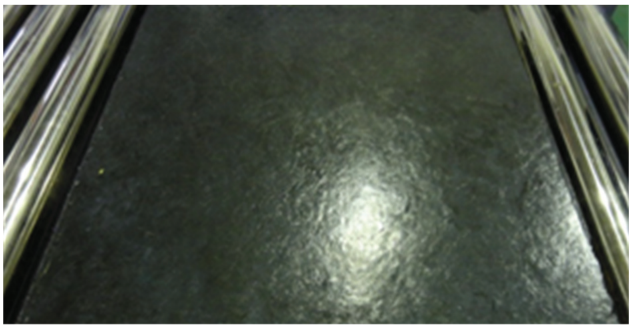

Fig. 1. Rough surface of CFRTP after cooling.

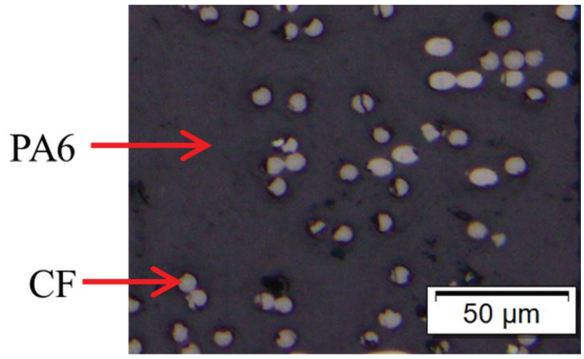

Fig. 2. Cross-sectional distribution of carbon fibers in CFRTP specimen.

relatively long and discontinuous fibers has an advantage in that it can mold even high-strength materials into complex shapes in a high-speed cycle [1].

Among the current issues with the LFT-D process is the surface roughness of finished products. In the LFT-D press-molding process, the high-temperature CFRTP surface immediately after release from the mold has almost the same smoothness as that of the mold surface. As the CFRTP cool, however, their surface roughness increases, as shown in **Fig. 1**: the arithmetic average roughness *Ra* of the CFRTP surface after cooling is 0.49 μm, approximately twice that of the mold surface ($Ra =$ 0.25 μm). One of the reasons for the surface roughness of CFRTP is the unevenly dispersed CFs in the thermoplastic resin. During the cooling process for CFRTP press-molded at high temperatures, the entire material thermally shrinks. Components made from a single material uniformly shrink when cooled, leading no adverse effects to a finished product except for the warpage or sink of the material caused by asymmetrical cooling. Conversely, composite materials like CFRTP contain different materials in their base material; hence, any difference in thermal shrinkage between the base and dispersed materials can cause roughness on the surface. In the LFT-D kneading process, where CFs with lengths of approximately 10 to 20 mm are kneaded with molten thermoplastic resin, it is not possible to knead the materials completely uniformly. Any non-uniform CF distribution caused in the above-mentioned kneading process can lead to a difference in shrinkage between the materials when thermally shrunk; hence, any non-uniform CF dispersion can accelerate the increase in surface roughness.

Although the surface roughness of CFRTP press-molded by the LFT-D technique is considered to be caused by thermal shrinkage, there are no studies available that have verified or quantitatively analyzed the validity of said mechanism; hence, there are no guidelines for molding CFRTP with excellent surface quality. High design standards are required for many actual industrial products; for instance, the surface quality applicable to automotive outer panels is called the Class A Surface to strictly control the surface quality [18]. Therefore, any CFRTP product molded by the LFT-D technique should have a surface roughness that is as small as possible. For the CFRTP resin, research and development efforts are under way regarding the methods for molding a product that will have an arithmetic average roughness $Ra =$ 10 nm or less [19]. Current CFRTP possess *Ra* values of approximately 500 nm; therefore, they are not applicable to automotive outer panels.

In this study, we aim to build a surface roughness generation estimation model for CFRTP by clarifying the mechanism for the CFRTP surface roughness generated in the cooling process after being press-molded using the LFT-D technique. We also attempt to construct a surface roughness estimation formula based on the above-mentioned surface roughness generation estimation model and finally propose guidelines for designing CFRTP with a low level of surface roughness.

2. Surface Roughness Generation Model for CFRTP Press-Molded by LFT-D

2.1. Cross-Sectional Features of CFRTP

The features of long and discontinuous fiber CFRTP press-molded by the LFT-D technique include a large difference in thermal shrinkage between CFs and thermoplastic resin. Comparison of their thermal expansion coefficients shows that CFs' thermal expansion coefficient is -0.4×10^{-6} 1/°C in the axial direction and 5.5×10^{-6} 1/°C in the diameter direction, and that of polyamide 6 (PA6), a thermoplastic resin, is 8×10^{-5} 1/°C [20]. PA6, with a thermal expansion coefficient approximately ten times larger than that of CFs, shrinks more when cooled.

Another feature of CFRTP press-molded by the LFT-D method is the uneven distribution of CFs in the material. CFRTP with continuous fibers, which is used for aircraft, consists of regularly laminated CFs or woven CF sheets. CFRTP with such CFs show only a small deviation in their internal CF distribution. Conversely, CFRTP press-molded by the LFT-D technique, which involves kneading CFs and thermoplastic resin by screws, inevitably show some deviation in the internal CF distribution. **Fig. 2** shows an optical microscopy image of the cross-section of CFRTP: white circular spots indicate the cross-sections of

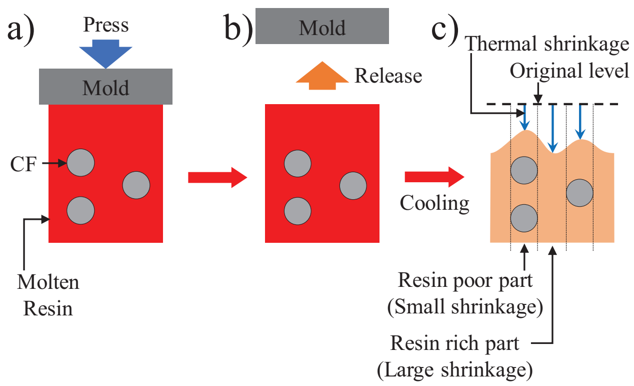

Fig. 3. Surface roughness generation model based on thermal shrinkage.

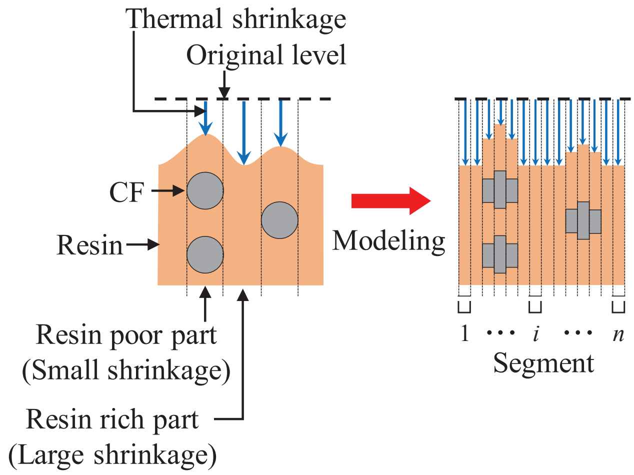

Fig. 4. Surface roughness calculation method by separating into small segments.

CFs, and the surrounding black areas are PA6. It is clear from said cross-sectional image of CFRTP that CFs are not uniformly distributed.

2.2. Concept for Surface Roughness Generation Model and Calculation Method

In this study, we have constructed a surface roughness generation model for cooled CFRTP surface roughness generated by the difference in thermal shrinkage between CFs and thermoplastic resin and by the unevenly distributed CFs in CFRTP. **Fig. 3** shows the concept of the surface roughness generation model.

During the press-molding of CFRTP by the LFT-D technique, a molten kneaded object is first press-molded, when CFs in the molded body are distributed as shown in **Fig. 3 a)**. After that, the molded body is released from the mold in a high-temperature state. Immediately after being released from the mold, CFRTP, which are still in a high-temperature state, do not thermally shrink and show a surface as smooth as that of the mold surface (**Fig. 3 b)**). Next, as the CFRTP cool, both the CFs and thermoplastic resin thermally shrink. However, because there is an approximately ten-fold difference in their shrinkage rate [20, 21], CF-rich areas shrink less and CF-poor or free areas shrink more (**Fig. 3 c)**). We have constructed a surface roughness generation model for CFRTP that takes these results into account.

We have devised a calculation method to quantitatively estimate the final surface roughness from the shrinkage amount of each of the fine vertical segments of the cross-section of CFRTP. In this calculation method, the cross-section of CFRTP is first divided into numerous segments, as shown in **Fig. 4**. Then, the quantities of CFs and thermoplastic resin that are present in such segments are determined, making it possible to calculate their respective longitudinal shrinkage amounts. Because the surface roughness can be analytically calculated from the segments' different shrinkage amounts, we consider it possible to estimate the surface roughness of a composite material from its cross-sectional data. In this study, we have validated the devised calculation method by quantitatively comparing the actual CFRTP surface roughness with the estimated surface roughness.

2.3. Thermal Shrinkage Rate of Thermoplastic Resin

In the surface roughness generation model proposed in this study, surface roughness is generated on CFRTP when the thermoplastic resin shrinks during the cooling process from high temperatures immediately after release from the mold to normal temperatures. The calculation method to estimate surface roughness on the proposed surface roughness generation model therefore requires the molding shrinkage rate ε of the thermoplastic resin during this cooling period at atmospheric pressure. We have calculated the shrinkage of the thermoplastic resin from the temperature and specific volume curve (PVT diagram). **Fig. 5** shows the PVT diagram of PA6, the thermoplastic resin material for CFRTP used in the verification tests. This diagram is based on data from Puffr et al. [22].

For instance, we can calculate the CFRTP shrinkage under the following conditions: the ambient pressure is 0.1 MPa; the CFRTP temperature is 152°C, the same as that of the mold when it starts to shrink; CFRTP are finally cooled down to room temperature. Under these test conditions, we read changes in the specific volume of CFRTP from the axis of the ordinate along the isobaric line of 0.1 MPa when the CFRTP cools to 25°C from 152°C, as shown in **Fig. 5**. We can read from the graph in **Fig. 5** that the specific volume of CFRTP is 0.93 cm^3/g at 152°C and 0.88 cm^3/g at 25°C. With these values denoted by a and b, respectively, the molding shrinkage rate ε can be expressed by Eq. (1):

$$\varepsilon = \frac{b^{\frac{1}{3}} - a^{\frac{1}{3}}}{b^{\frac{1}{3}}} = 1 - \left(\frac{a}{b}\right)^{\frac{1}{3}} \quad \text{. . . . . (1)}$$

While the molding shrinkage rate ε indicates a one-dimensional length ratio, specific volume indicates a three-dimensional value: hence, the multiplier $1/3$ is used

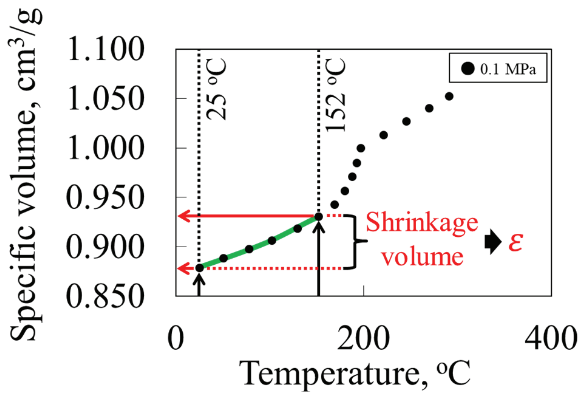

Fig. 5. Pressure-volume-temperature (PVT) diagrams of PA6. The shrinkage factor can be calculated by the specific volume at high and cooled temperatures.

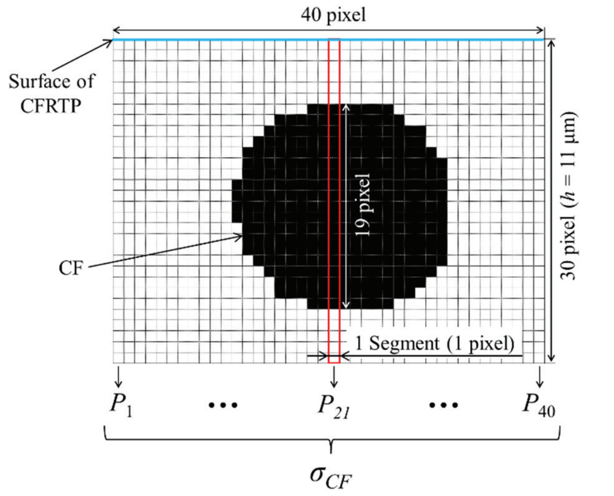

Fig. 6. Sample binarized BMP image of CFRTP cross-section.

in Eq. (1). By substituting the specific volumes read from **Fig. 5** into Eq. (1), we can obtain the molding shrinkage rate $\varepsilon = 0.018$ for CFRTP that have been cooled down to 25°C from 152°C.

2.4. Distribution of Carbon Fibers in CFRTP

The surface roughness estimation calculation method proposed in this study represents the degree of uneven distribution of CFs in the cross-section of CFRTP with the sample standard deviation σ_{CF} of CFs contained in the segments into which the cross-section is divided, as well as by their probability density function $f(x, \sigma_{CF}, \mu)$. In this study, we have sought σ_{CF} directly from the cross-sectional image of CFRTP, as shown in **Fig. 2**.

To observe the cross-section of CFRTP, we cut a CFRTP specimen with a fine cutter and embed-polished the cross-section of the cut specimen. After that, we captured its cross-sectional images with an optical microscope. Finally, we binarized the captured cross-sectional images and stored them as bit map data. Bit map image data built with 0 or 1 for each pixel should be suitable for analyses using the surface roughness estimation calculation method.

Figure 6 shows a part of the cross-sectional image as acquired by its binarization: an image at a depth of 11 μm from the CFRTP surface, 30×40 pixels: each section divided by dotted lines represents one pixel; the black area represents CFs, and the white area is resin. We have vertically segmented this image as shown in **Fig. 4**. In the tests, we have analyzed the image by assuming the width of one segment is one pixel. Next, we have calculated the pixel number P_i of the CF part in the i-th segment: a parameter corresponding to the volume of CFs present in each segment; for instance, the black color pixel number P_{21} in the 21st segment enclosed by a square is 19 pixels. We have calculated P_i for every segment; taking **Fig. 6** for example, we have calculated P_i from P_1 through P_{40}.

We have calculated the sample standard deviation σ_{CF} of P_i from Eq. (2).

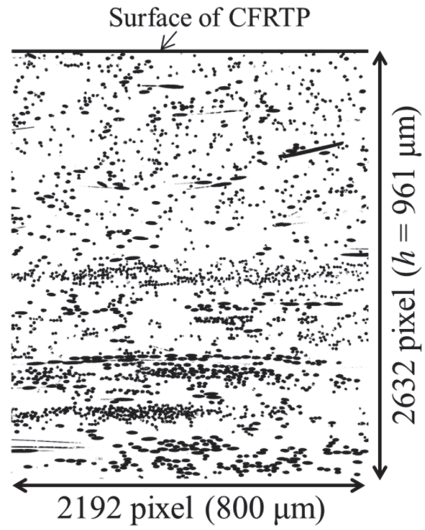

Fig. 7. Binarized BMP image of CFRTP cross-section for calculation of surface roughness.

$$\sigma_{CF} = \sqrt{\frac{1}{n-1}\sum_{i=1}^{n}(P_i - \mu)^2}, \quad \ldots \ldots \ldots \quad (2)$$

where μ denotes the average of P_i and n is the number of segments in the binarized cross-sectional image: $n = 40$ in the case of **Fig. 6**. In conducting actual analyses, we have calculated σ_{CF} from the binarized cross-sectional image with 2632×2192 pixels, as shown in **Fig. 7**: 2632×2192 pixels corresponds to the actual size of 961×800 μm. In conducting the estimation calculations for the surface roughness generated by thermal shrinkage, we have averaged the σ_{CF} acquired from three different binarized cross-sectional images.

Using the sample standard deviation σ_{CF} of the CF volume contained in each segment and from the average μ of P_i, we have calculated a probability density function $f(x, \sigma_{CF}, \mu)$ that takes a Gaussian distribution, as shown in Eq. (3).

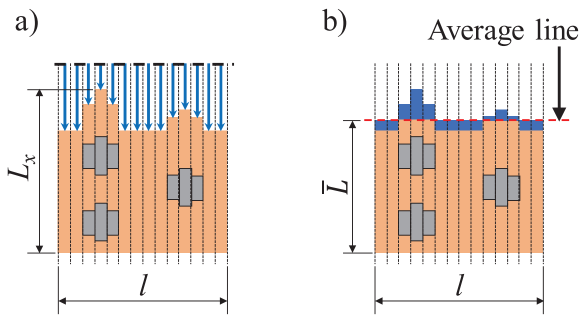

Fig. 8. Schematics of (a) length of each segment L_x and (b) average length of L_x.

$$f(x, \sigma_{CF}, \mu) = \frac{1}{\sqrt{2\pi\sigma_{CF}^2}} \left\{ \exp\left(-\frac{(x-\mu)^2}{2\sigma_{CF}^2} \right) \right\}, \quad (3)$$

where x denotes the pixel number of the CFs contained in each segment; in the case of **Fig. 6**, it can be any number from 0 up to a maximum of 30.

2.5. Post-Cooling Shrinkage in Length

With x denoting the pixel number of CFs in a segment, we have calculated the post-shrinkage length L_x from Eq. (4).

$$L_x = \{x + (h_p - x) \times (1 - \varepsilon)\} \times r \quad . \; . \; . \; . \; . \quad (4)$$

where h_p denotes the longitudinal pixel number contained in one segment and r is the length per pixel in actual space. In the case of **Fig. 6**, h_p is 30 pixels and r is 0.36 μm/pixel. Given that PA6 has a thermal expansion coefficient that is approximately ten times larger than that of CFs, we have ignored the shrinkage of CFs in this study.

2.6. Theoretical Formula for Surface Roughness Estimation

Using Eqs. (2)–(4), we can derive a theoretical formula for estimating the arithmetic average roughness Ra generated on the CFRTP surface. The arithmetic average roughness can be obtained by dividing the area enclosed by the center line and the roughness curve by the evaluation length [23]. First, we seek the absolute value for the difference between L_x and its average value $\bar{L}$ and multiply it by the probability density function $f(x, \sigma_{CF}, \mu)$; then, the difference $(L_x - \bar{L})$ is weighted according to the amount of CFs in each segment. These values are then multiplied by the evaluation length l and summed up from $x = 0$ to h_p, which denotes that the entire segment is filled with CFs, to obtain the area turned deeper color in **Fig. 8**. Finally, the area is divided by l to obtain the arithmetic average roughness Ra. This process can be expressed by Eq. (5).

$$Ra = \frac{1}{l} \sum_{x=0}^{h_p} \{ |L_x - \bar{L}| \times f(x, \sigma_{CF}, \mu) \times l \} \; . \; . \; . \quad (5)$$

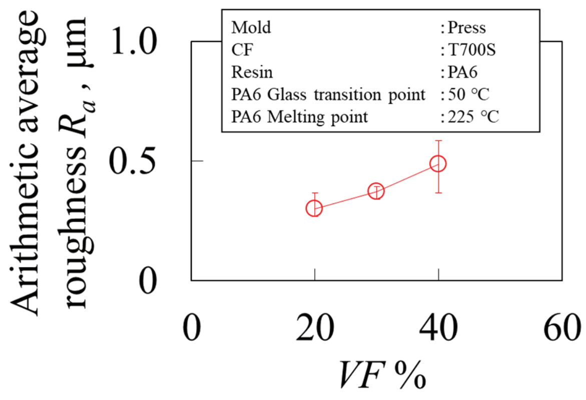

Fig. 9. Surface roughness of CFRTP with variety of carbon fiber volume fractions.

3. Experimental Results

3.1. Surface Roughness of CFRTP with Various Carbon Fiber Volume Fractions

To validate the surface roughness generation model and its calculation method proposed in this study, we have first measured the arithmetic average surface roughness of actual CFRTP specimens. We press-molded CFRTP specimens that contain PA6 as the thermoplastic resin and TORAY-made T700SC as CFs.

We measured the arithmetic average surface roughness of three CFRTP specimens with different CF volume fractions (VFs) with a tracer-type surface roughness meter SV-3100 made by MITSUTOYO Inc. We measured the arithmetic average roughness at six points on the CFRTP surface per specimen and averaged them to obtain the measurement results. **Fig. 9** shows the arithmetic average surface roughness of three specimens having different CFVFs. The measurement results show that as the CFVF of the specimen increases, its arithmetic average surface roughness increases accordingly.

3.2. Surface Roughness Estimation Using Theoretical Formula

We have analyzed cross-sectional images of the CFRTP specimens used to measure the arithmetic average surface roughness using the proposed surface roughness estimation calculation method, as shown in **Fig. 9**. As the specimens we have used for the measurements have different CFVFs, we have validated the proposed surface roughness generation model and surface roughness estimation calculation method by comparing the analysis results with the trends shown in **Fig. 9**.

Figure 10 shows the analysis results using the surface roughness estimation calculation method: the circled data points in **Fig. 10** indicate the actual CFRTP surface roughness shown in **Fig. 9**. For the pre-shrinkage segment length h_p or corresponding h used for Eq. (4) in the surface roughness estimation formula we have derived, we have used four different values as parameters for the analyses. The analysis results shown in **Fig. 10** demon-

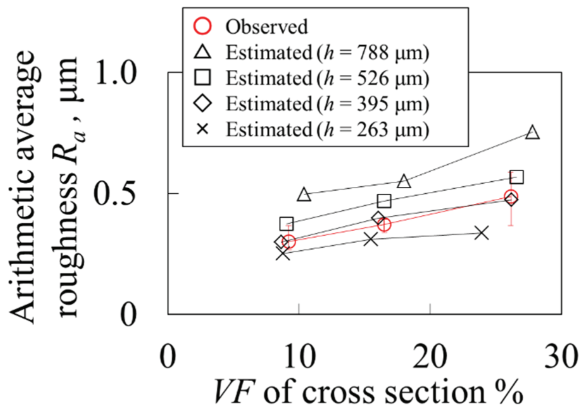

Fig. 10. Calculated surface roughness with variety of carbon fiber volume fractions.

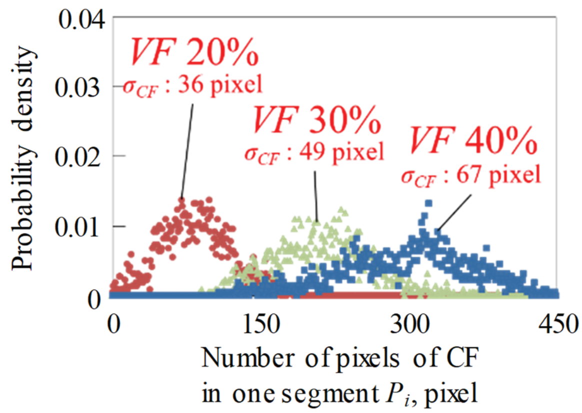

Fig. 11. Broad distribution of probability density with increase in carbon fiber volume fraction.

strate that whatever value h may be, the estimated surface roughness value increases as the CFVF increases: this agrees with the results obtained from the actual CFRTP specimens shown in **Fig. 9**. We have also calculated the rate of increase between the surface roughness and the CFVF from the inclination of the regression line. While the inclination of the regression line for the actual CFRTP is 0.011, that of the calculated surface roughness line is 0.010 on average, i.e., they are in good agreement with each other. When $h = 395$ μm, the estimated surface roughness value is almost the same as the experimental value, with an average deviation of 3%; this is very good agreement.

4. Discussion

4.1. Increase in Carbon Fiber Volume Fraction and its Effects on Surface Roughness

We can see from the surface roughness estimation Eq. (5) that as the standard deviation of the CF amount present in one segment σ_{CF} increases, the estimated arithmetic average surface roughness value increases accordingly. So long as the surface roughness generation model and the surface roughness estimation formula accurately represent the actual surface roughness generation mechanism, therefore, we may consider that the increase in surface roughness of actual CFRTP shown in **Fig. 9** is due to the increase in the standard deviation of the CF amount present in the specimens, σ_{CF}.

Figure 11 shows the probability density distributions of P_i for $h = 395$ μm as acquired from the cross-sectional images of actual CFRTP specimens. We can see from **Fig. 11** that as the CFVF increases, the average P_i value increases and the probability density distribution spreads out. These findings from the cross-sectional images of actual CFRTP verify that the standard deviation of the CF amount present in an actual specimen σ_{CF} should increase as the amount of CFs increases.

Any increase in the CFVF means an increase in the CF amount present in the CFRTP specimen with the same volume. Accordingly, the increase in the amount of CFs present in one segment seems to lead to an increase in the average CF amount. Conversely, the distribution of the amount of CFs in one segment spreads out as the CFVF increases, probably because as the expected value for the carbon fiber amount present in one segment increases, the number of combinations of the cases where CFs are actually present or not increases. For instance, if the total amount of CFs doubles, the expected value for the amount of CFs present in one segment also doubles.

However, because the amount of CFs actually present in the segment depends on a random probability distribution, some segments may contain more CFs than the increased expectation value, and others will have fewer CFs. Therefore, any increase in the CFVF seems to spread out the probability density distribution.

In other words, we may be able to prevent the standard deviation of the amount of CFs σ_{CF} from increasing with an increase in CFVF if we could knead them enough so that any increased amount of CFs could be dispersed in the same way as in the case of smaller amounts of CFs. Stochastically, however, it is difficult to maintain the standard deviation of the amount of CFs, σ_{CF}, as described above. The said difficulty could be solved by increasing the kneading temperature to decrease the viscosity of thermoplastic resin or by kneading for a longer time in the case of any increased CFVF, for instance.

The findings shown in **Figs. 10** and **11** verify that decreasing the standard deviation of the amount of CFs, σ_{CF}, should be effective to reduce the arithmetic average surface roughness. σ_{CF} is a parameter that depends on the CFRTP molding conditions, such as molding temperature and molding pressure, as well as on the properties of the object kneaded from CFs and thermoplastic resin, such as molding shrinkage ε and the CFVF. This study finds that it is important to determine the kneading conditions, viscosity of molten thermoplastic resin, and press-molding conditions to achieve uniform distribution of CFs.

Regarding the depth h in Eq. (4), theoretically it refers to the entire depth of the cross-section of the CFRTP, but practically, CFs located sufficiently deep with respect to

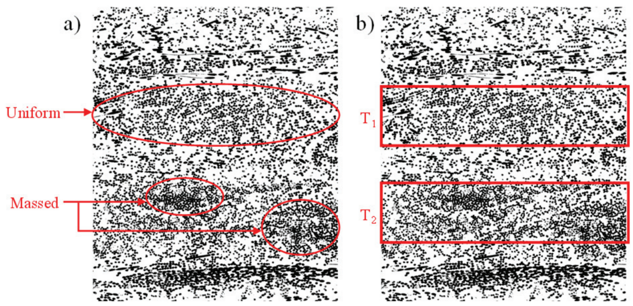

Fig. 12. Binarized cross-sectional image of a CFRTP specimen with a volume fraction of 40%.

the CFRTP surface seem to have little effect on the surface roughness. There are some reports [24, 25] that report success in reducing the surface roughness of CF thermosetting resin to approximately one-tenth of the original amount by providing a resin layer on the surface that is tens of μm thick. There are no studies available, however, on the depth of CFs present in thermoplastic resin that will affect the surface roughness of the CFRTP. Conversely, given that thermoplastic resin is generally known to have a larger molding shrinkage than thermosetting resin, it can be reasonable that the estimated surface roughness in this study had a very small average deviation of 3% from the experimental values in the case of $h = 395$ μm. These findings tell us that in the case of CFRTP whose CF distribution is not greatly affected by the depth, the effective depth in the surface roughness estimation calculation is approximately 400 μm. Conversely, in molding CFRTP whose CF distribution in the depth direction greatly varies because of demands for material strength and/or adhesive property, it may be more important to include the effects of the depth on the surface roughness; hence, there is a need for detailed studies on the effective depth.

4.2. Effects of Carbon Fiber Mass on Surface Roughness

Figure 12 shows a binarized cross-sectional image of CFRTP with a CFVF of 40%, from which we can recognize the areas where CFs are relatively uniformly dispersed and where they are massed together. To quantitatively clarify the effects of CF distributions on the surface roughness, we have extracted two regions, T_1 and T_2, from one cross-section and have calculated the arithmetic average roughness from Eq. (5). T_1 and T_2 represent the layers where we can visually observe CFs uniformly distributed and massed together, respectively.

The resultant estimated arithmetic average roughness is 0.37 μm for T_1, 14% smaller than the value for T_2 (0.43 μm), which demonstrates that distributing CFs uniformly without consideration of mass is effective for molding CFRTP with excellent properties.

Carbon fibers mass together partly because CFs as a product are in the state of a filament or a tow, where several tens of thousands of single fibers are adhered together. Both filament and tow, although different from each other with respect to twisting and in the number of included fibers, are in the state where multiple single fibers are adhered together into one fiber with a resin called a sizing agent. Carbon fibers made of a single fiber, an ultrafine fiber of $\phi 7$ μm in diameter, are easily scattered. They possess carbon-derived conductivity, so that when attached to a circuit board or the wiring part of an electrical appliance, they can cause a malfunction of such an appliance. The sizing treatment for CFs is taken to prevent them from scattering. Carbon fibers that are drawn into the kneading screws in the LFT-D process are in a state where several tens of thousands of fibers are adhered together. The sizing agent, a resin material, is melted at a high temperature and flows when kneaded. In view of the facts that CFs are massed together in their initial state and that both sizing agent and molten thermoplastic resin have relatively large viscosity, to achieve an uniform CF distribution, we need to take the following measures in the kneading process: kneading with a large shearing force, kneading for a sufficiently long time, and kneading under high-temperature conditions.

In this study, we found that to mold CFRTP with suitable properties, we need to secure an uniform CF distribution at a depth of approximately 400 μm from the surface. For instance, as it is known in the heat and cool molding technique that a resin-rich layer is generated on the outermost surface, we may expect to be able to mold CFRTP with excellent surface glossiness by incorporating the said molding technique into the LFT-D press-molding process. It could be a more practical technique to insert a resin film or a prepreg containing woven continuous fibers between the mold and the CFRTP kneaded body [26]. The findings of this study suggest that this technique can contribute to distributing CFs uniformly on the surface, thus improving the surface roughness.

The surface roughness generation model proposed in this study is a generic model, so that it can be practically applied. For instance, we can estimate surface roughness using finite element analyses for thermal shrinkage. Use of the finite element analyses, where thermal shrinkage in the horizontal direction (which the proposed estimation formula does not take into account) is considered, will enable high-accuracy analyses. We should note, however, that it would take a huge cost to calculate the surface roughness of a model reflecting actual CF distributions. Because the proposed method can easily calculate estimated surface roughness from the optical microscopy images of the cross-sections of a specimen, it should be widely applicable to analyze the main causes of surface roughness generation.

5. Conclusion

This study aimed to clarify the mechanism for generating roughness on the surface of high-temperature press-molded CFRTP in its cooling process as well as to propose an estimation calculation method. In this study, we have constructed a model where in particular any difference in thermal shrinkage between thermoplastic resin and CFs and uneven distributions of CFs will affect the surface roughness generation.

For the estimated calculations of surface roughness, we have devised a shrinkage model assuming that thermal shrinkage occurs in each vertically divided segment. Based on this shrinkage model, we have derived a theoretical formula to estimate the arithmetic average roughness using the standard deviation of the amount of CFs σ_{CF}, the average value μ, and the probability density function $f(x, \sigma_{CF}, \mu)$.

We have measured the surface roughness of CFRTP actually molded by the LFT-D technique to determine that the arithmetic average roughness increases in accordance with the CFVF. We have compared the above-mentioned experimental results with values obtained from the proposed estimation formula to find that the inclinations of the respective regression lines are 0.011 and 0.010, in good agreement with each other. In addition, we have conducted estimation calculations using an effective depth of 395 μm for thermal shrinkage that will affect the surface roughness to prove that the surface roughness can be estimated with an average deviation of 3% from the actual measurements.

The surface roughness estimation formula derived in this study shows that the surface roughness increases with an increase in the standard deviation of the amount of CFs in the segments, which agrees with the observation results for the cross-section of actual CFRTP. Therefore, the surface roughness generation model and its estimation formula proposed in this study can be widely applied in practical applications.

References:

[1] M. Yamane, "Thermoplastic CFRP technology collection, Tribology of diamond-like carbon films: recent progress and future prospects," Science & Technology Co., Ltd., 2015 (in Japanese).

[2] R. Sawaoka et al., "CFRP/CFRTP no kakougijutu to seinouhyouka (2nd edition)," S&T Publishing inc., 2012 (in Japanese).

[3] C. Soutis, "Carbon fiber reinforced plastics in aircraft construction," Mat. Sci. Eng. A, Vol.412, Issues 1-2, pp. 171-176, 2005.

[4] C. Soutis, "Fibre reinforced composites in aircraft construction," Progress in Aerospace Sci., Vol.41, Issue 2, pp. 143-151, 2005.

[5] A. Kitano, "Characteristics of Carbon-Fiber-Reinforced Plastics (CFRP) and Associated Challenges – Focusing on Carbon-Fiber-reinforced Thermosetting Resins (CFRTS) for Aircraft," Int. J. Automation Technol., Vol.10, No.3, pp. 300-309, 2016.

[6] Y. Kurihara, "The role of aluminum in automotive weight reduction – Part I," JOM, Vol.45, Issue 11, pp. 32-33, 1993.

[7] M. K. Kulekci, "Magnesium and its alloys applications in automotive industry," Int. J. Adv. Manuf. Technol., Vol.39, Issues 9-10, pp. 851-865, 2008.

[8] Europe Union, "Regulation (EU) No 333/2014 of the European parliament and of the council," Official J. of the European Union, pp. L103/15-L103/21, 2014.

[9] H. Helms and U. Lambrecht, "The potential contribution of light-weighting to reduce transport energy consumption," Int. J. Life Cycle Assess., Vol.12, No.1, pp. 1-7, 2007.

[10] Y. Kurihara, "The role of aluminum in automotive weight reduction – Part II," JOM, Vol.46, Issue 2, pp. 33-35,1994.

[11] L. W. Cheah, "Cars on a diet: The material and energy impacts of passenger vehicle weight reduction in the U.S.," Ph.D. thesis in Engineering Systems, Massachusetts Institute of Technology, pp. 1-121, 2010.

[12] W. Krause, F. Henning, S. Tröster, O. Geiger, and P. Eyerer, "LFT-D – A process technology for large scale production of fiber reinforced thermoplastic components," J. Thermoplastic Comp. Mat., Vol.16, No.4, pp. 289-302, 2003.

[13] F. Henning, H. Ernst, R. Brussel, O. Geiger, and W. Krause, "LFTs for automotive applications," REINFORCED Plastics, Vol.49, Issue 2, pp. 24-33, 2005.

[14] O. Geiger, F. Henning, P. Eyerer, R. Brussel, and H. Ernst, "LFT-D: materials tailored for new applications," Reinforced Plastics, Vol.50, No.1, pp. 30-35, 2006.

[15] M. Schemme, "LFT – development status and perspectives," Reinforced Plastics, Vol.52, Issue 1, pp. 38-43, 2008.

[16] F. W. J. van Hattum, J. P. Nunes, and C. A. Bernardo, "A theoretical and experimental study of new towpreg-based long fibre thermoplastic composites," Composites Part A: Applied Science and Manufacturing, Vol.36, Issue 1, pp. 25-32, 2005.

[17] J. Markarian, "Long fibre reinforced thermoplastics continue growth in automotive," Plastics, Additives and Compounding, Vol.9, Issue 2, pp. 20-22, 24, 2007.

[18] R. Hsakou, "Curvature: the relevant criterion for Class A surface quality," JEC Composites Magazine, No.43, pp. 105-108, 2006.

[19] N. Boyard, C. Serré, and M. Vayer, "A Physical Approach to Define a Class A Surface in Polymer Thermosetting Composite Materials," J. Appl. Polymer Sci., Vol.103, No.1, pp. 451-461, 2007.

[20] T. Kikutani and K. Takemura, "Illustration: Plastic mold material," Morikita Publishing Co., Ltd., pp. 74-81, 2011 (in Japanese).

[21] T. Kyono and K. Takahashi, "Theoretical Investigation of the Thermal Expansion Coefficients of Unidirectional Carbon Fiber Composites," J. Soc. Mat. Sci., Vol.38, Issue 426, pp. 307-311, 1989 (in Japanese).

[22] R. Puffr and V. Kubánek, "Lactam-based Polyamides Volume II Modification, Technology and Application," CRC Press, pp. 187-188, 1991.

[23] Japanese Industrial Standards, JIS B 0601:2013, "Geometrical Product Specifications (GPS) – Surface texture: Profile method – Terms, definitions and surface texture parameters," 2013.

[24] http://www.kenkai.jaxa.jp/research/pastres/cfrp.html [Accessed July 28, 2019]

[25] T. Kamiya, S. Utsunomiya, K. Komatsu, and R. Shimizu, "Improvement of the CFRP composite mirror surface using a replica method," Proc. of 18th Int. Conf. on composite Mat., pp. 1-6, 2011.

[26] T. Yoneyama, D. Tatsuno, K. Kawamoto, and M. Okamoto, "Effect of press slide speed and stroke on cup forming using a plain-woven carbon fiber thermoplastic composite sheet," Int. J. Automation Technol., Vol.10, No.3, pp. 381-391, 2016.

Name:
Motoyuki Murashima

Affiliation:
Assistant Professor, Department of Micro-Nano Mechanical Science and Engineering, Graduate School of Engineering, Nagoya University

Address:
Furo-cho, Chikusa-ku, Nagoya, Aichi 464-8603, Japan

Brief Biographical History:

2012- Ph.D. Student, Graduate School of Engineering, Nagoya University
2014- Visiting Ph.D. Student, MADL Lab., University of Toronto
2016- Assistant Professor, Nagoya University

Main Works:

- "Intelligent tribological surfaces: from concept to realization using additive manufacturing," Int. J. Mech. Mater. Des., Vol.15, No.4, pp. 1-10, 2019.
- "Effect of oxygen on degradation of defects on ta-C coatings deposited by filtered arc deposition," Surf. & Coat. Technol., Vol.362, pp. 200-207, 2019.

Membership in Academic Societies:

- Japanese Society of Tribologists (JAST)
- Japan Society of Mechanical Engineers (JSME)
- Japan Society for Precision Engineering (JSPE)

Name:
Takaharu Murooka

Affiliation:
Master Course Student, Department of Mechanical Science and Engineering, Graduate School of Engineering, Nagoya University

Address:
Furo-cho, Chikusa-ku, Nagoya, Aichi 464-8603, Japan

Brief Biographical History:
2012- Department of Mechanical and Aerospace Engineering, Nagoya University
2016- Graduate School of Engineering, Nagoya University

Main Works:
- Designed surface of carbon fiber reinforced plastics

Name:
Noritsugu Umehara

Affiliation:
Professor, Department of Micro-Nano Mechanical Science and Engineering, Graduate School of Engineering, Nagoya University

Address:
Furo-cho, Chikusa-ku, Nagoya, Aichi 464-8603, Japan

Brief Biographical History:
1995- Associate Professor, Tohoku University
2001- Professor, Nagoya Institute of Technology
2003- Professor, Nagoya University

Main Works:
- "Clarification of relationship between friction coefficient and transformed layer of CNx coating by in-situ spectroscopic analysis," Tribology Int., Vol.93, Part B, pp. 660-665, 2016.

Membership in Academic Societies:
- Japan Society of Mechanical Engineers (JSME)
- Japanese Society of Tribologists (JAST)
- Japan Society for Precision Engineering (JSPE)

Name:
Takayuki Tokoroyama

Affiliation:
Associate Professor, Department of Micro-Nano Mechanical Science and Engineering, Graduate School of Engineering, Nagoya University

Address:
Furo-cho, Chikusa-ku, Nagoya, Aichi 464-8603, Japan

Brief Biographical History:
2006- Assistant Professor, Nagoya University
2014- Associate Professor, Akita University
2017- Associate Professor, Nagoya University

Main Works:
- "Collecting micrometer-sized wear particles generated between DLC/DLC surfaces under boundary lubrication with electric field," JSME Mechanical Engineering Letters, Vol.4, 18-00089, 2018.

Membership in Academic Societies:
- Japan Society of Mechanical Engineers (JSME)
- Japanese Society of Tribologists (JAST)
- Japan Society of Applied Physics (JSAP)
- Japan Society of Refrigerating and Air Conditioning Engineers (JSRAE)
- Japan Society for Abrasive Technology (JSAT)